The Astrophysical Journal, 694:174–182, 2009 March 20 doi:10.1088/0004-637X/694/1/174
© 2009. The American Astronomical Society. All rights reserved. Printed in the U.S.A.

THE WHOLE EARTH BLAZAR TELESCOPE CAMPAIGN ON THE INTERMEDIATE BL LAC OBJECT 3C 66A IN 2007–2008*

M. Böttcher[1], K. Fultz[1], H. D. Aller[2], M. F. Aller[2], J. Apodaca[3], A. A. Arkharov[4], U. Bach[5], R. Bachev[6], A. Berdyugin[7], C. Buemi[8], P. Calcidese[9], D. Carosati[10], P. Charlot[11,12], S. Ciprini[13], A. Di Paola[14], M. Dolci[15], N. V. Efimova[4], E. Forné Scurrats[16], A. Frasca[8], A. C. Gupta[17], V. A. Hagen-Thorn[18,19], J. Heidt[20], D. Hiriart[21], T. S. Konstantinova[18], E. N. Kopatskaya[18], A. Lähteenmäki[22], L. Lanteri[23], V. M. Larionov[18,19], J.-F. Le Campion[11,12], P. Leto[24], E. Lindfors[7], E. Marilli B. Mihov[6], E. Nieppola[22], K. Nilsson[7], J. M. Ohlert E. Ovcharov[26], P. Pääkkönen[27], M. Pasanen[7], B. Ragozzine[1], C. M. Raiteri[23], J. A. Ros[28], A. Sadun[3], A. Sanchez[29], E. Semkov[6], M. Sorcia[30], A. Strigachev[6], L. Takalo[7], M. Tornikoski[22], C. Trigilio[8], G. Umana[8], A. Valcheva[6], M. Villata[23], A. Volvach[31], J.-H. Wu[32], and X. Zhou[32]

[1] Astrophysical Institute, Department of Physics and Astronomy, Clippinger 339, Ohio University, Athens, OH 45701, USA
[2] Department of Astronomy, University of Michigan, 830 Dennison Building, Ann Arbor, MI 48109-1042, USA
[3] Department of Physics, University of Colorado Denver, Campus Box 157, P.O. Box 173364, Denver, CO 80217-3364, USA
[4] Pulkovo Observatory, Pulkovskoye Shosse, 65, 196140, St. Petersburg, Russia
[5] Max-Planck-Institut für Radioastronomie, Radioobservatorium Effelsberg, Max-Planck-Straße 28, D-53902 Bad Münstereifel-Effelsberg, Germany
[6] Institute of Astronomy, Bulgarian Academy of Sciences, 72 Tsarigradsko shosse Blvd., 1784 Sofia, Bulgaria
[7] Tuorla Observatory, University of Turku, 21500 Piikkiö, Finland
[8] Osservatorio Astrofisico di Catania, Viale A. Doria 6, I-95125 Catania, Italy
[9] Osservatorio Astronomico della Regione Autonoma Valle d'Aosta, Italy
[10] Osservatorio di Armenzano, Assisi, Italy
[11] Université de Bordeaux, Observatoire Aquitain des Sciences de l'Univers, Floirac, France
[12] CNRS, Laboratoire d'Astrophysique de Bordeaux-UMR 5804, Floirac, France
[13] Osservatorio Astronomico, Università di Perugia, Via B. Bonfigli, I-06126 Perugia, Italy
[14] Istituto Nazionale di Astrofisica (INAF), Osservatorio Astronomico di Roma, Via Frascati, Monteporzio Cantone, Roma, Italy
[15] Istituto Nazionale di Astrofisica (INAF), Osservatorio Astronomico di Teramo, Via Maggini, Teramo, Italy
[16] Code MPC B29, Astronomical Observatory L'Ampolla, Tarragona, Spain
[17] Aryabhatta Research Institute of Observational Sciences (ARIES), Manora Peak, Nainital-263 129, India
[18] Astronomical Institute, St. Petersburg State University, Universitetsky pr. 28, Petrodvoretz, 198504 St. Petersburg, Russia
[19] Isaac Newton Institute of Chile, St. Petersburg Branch, 198504 St. Petersburg, Russia
[20] Landessternwarte Heidelberg-Königstuhl, Königstuhl, D-69117 Heidelberg, Germany
[21] Instituto de Astronomía, Universidad Nacional Autónoma de México, Apdo. Postal 877, 22800 Ensenada, B.C., Mexico
[22] Metsähovi Radio Observatory, Helsinki University of Technology TKK, Metsähovintie 114, 02540 Kylmälä, Finland
[23] Istituto Nazionale di Astrofisica (INAF), Osservatorio Astronomico di Torino, Via Osservatorio 20, I-10025 Pino Torinese, Italy
[24] INAF, Instituto di Radioastronomia, Sezione di Noto, Italy
[25] Michael Adrian Observatory, Astronomie-Stiftung Trebur, Fichtenstraße 7, D-65468 Trebur, Germany
[26] Sofia University "St. Kliment Ohridski," Faculty of Physics, 5 James Bourchier Blvd., 1164 Sofia, Bulgaria
[27] Department of Physics and Mathematics, University of Joensuu, Joensuu, Finland
[28] Agrupaciòn Astronomica de Sabadell, Sabadell 08200, Spain
[29] Gualba Observatory, MPC 442, Barcelona, Spain
[30] Instituto de Astronomía, Universidad Nacional Autónoma de México, Apdo. Postal 70-264, 04510 México, D.F., Mexico
[31] Crimean Astrophysical Observatory, Naunchy, Crimea 98409, Ukraine
[32] National Astronomical Observatories, Chinese Academy of Sciences, 20A Datun Road, Beijing 100012, China
Received 2008 September 8; accepted 2008 December 18; published 2009 March 13

ABSTRACT

Prompted by a high optical state in 2007 September, the Whole Earth Blazar Telescope consortium organized an intensive optical, near-IR (*JHK*) and radio observing campaign on the intermediate BL Lac object 3C 66A throughout the fall and winter of 2007–2008. In this paper, we present data from 28 observatories in 12 countries, covering the observing season from late 2007 July through 2008 February. The source remained in a high optical state throughout the observing period and exhibited several bright flares on timescales of ∼10 days. This included an exceptional outburst around 2007 September 15–20, reaching a peak brightness at $R \sim 13.4$. Our campaign revealed microvariability with flux changes up to $|dR/dt| \sim 0.02$ mag hr^{-1}. Our observations do not reveal evidence for systematic spectral variability in the overall high state covered by our campaign, in agreement with previous results. In particular, we do not find evidence for spectral hysteresis in 3C 66A for which hints were found in an earlier campaign in a somewhat lower flux state. We also did not find any evidence for spectral lags in the discrete correlation functions between different optical bands. We infer a value of the magnetic field in the emission region of $B \sim 19 \quad e_B^{2/7}\, \tau_h^{-6/7}\, D_1^{13/7}$ G, where e_B is the magnetic field equipartition fraction, τ_h is the shortest observed variability timescale in units of hours, and D_1 is the Doppler factor in units of 10. From the lack of systematic spectral variability, we can derive an upper limit on the Doppler factor, $D \leqslant 28 \quad \tau_h^{-1/8}\, e_B^{3/16}$. This is in perfect agreement with superluminal motion measurements with the VLBI/VLBA of $\beta_{\rm app} \leqslant 27$ and argues against models with very high Lorentz factors of $\Gamma \gtrsim 50$, required for a one-zone

synchrotron-self-Compton interpretation of some high-frequency-peaked BL Lac objects detected at TeV γ-ray energies.

Key words: BL Lacertae objects: individual (3C 66A) – galaxies: active – gamma rays: theory – radiation mechanisms: non-thermal

Online-only material: color figures

1. INTRODUCTION

Blazars are the most violent class of active galactic nuclei (AGNs), consisting of flat-spectrum radio quasars (FSRQs) and BL Lac objects. They exhibit rapid variability down to timescales as short as a few minutes (Aharonian et al. 2007; Albert et al. 2007b). Their observed flux is dominated by a nonthermal continuum exhibiting two broad spectral bumps: a low-frequency bump from radio to UV–X-ray frequencies, and a high-frequency component from X-ray to γ-rays.

In the framework of relativistic jet models, the low-frequency (radio–optical/UV) emission from blazars is interpreted as synchrotron emission from nonthermal electrons in a relativistic jet. The high-frequency (X-ray–γ-ray) emission could either be produced via Compton upscattering of low-frequency radiation by the same electrons responsible for the synchrotron emission (leptonic jet models; for a recent review see, e.g., Böttcher 2007), or due to hadronic processes initiated by relativistic protons co-accelerated with the electrons (hadronic models, for a recent discussion see, e.g., Mücke & Protheroe 2001; Mücke et al. 2003).

The blazar 3C 66A (= 0219 + 428) is classified as a low-frequency-peaked BL Lac object (LBL), a class also commonly referred to as radio selected BL Lac objects. Its nonthermal low-frequency spectral component extends from radio frequencies through soft X-rays and typically peaks in the optical frequency range. The high-frequency component seems to peak in the multi-MeV–GeV energy range. Since its optical identification by Wills & Wills (1974), 3C 66A has been the target of many radio, IR, optical, X-ray, and γ-ray observations in the past, although it is not as regularly monitored at radio frequencies as many other blazars due to problems with source confusion with the nearby radio galaxy 3C 66B (6.′5 from 3C 66A), in particular at lower (4.8 and 8 GHz) frequencies (Aller et al. 1994; Takalo et al. 1996).

To date, about two dozen blazars have been detected at very high energies (greater than 100 GeV) with ground-based air Čerenkov telescope facilities. Until very recently, all TeV blazars belonged to the subclass of high-frequency-peaked BL Lac objects (HBLs). However, the recent detections of the intermediate BL Lac object W Comae (Acciari et al. 2008), the LBL BL Lacertae (Albert et al. 2007a), and even the flat-spectrum radio quasar 3C 279 (Albert et al. 2008) demonstrate the potential to extend the extragalactic TeV source list to all classes of blazars, in particular intermediate and LBLs with lower νF_ν peak frequencies in their broadband spectral energy distributions (SEDs).

3C 66A has been suggested for quite some time as a promising candidate for detection by the new generation of atmospheric Čerenkov telescope facilities such as MAGIC or VERITAS (e.g., Costamante & Ghisellini 2002) (it is too far north in the sky to be observed by HESS), and intensive observations of 3C 66A by the VERITAS collaboration have recently resulted in the significant detection of very high energy (VHE) γ-ray emission from 3C 66A in 2008 September–October (Swordy et al. 2008).

In the optical, 3C 66A is generally observed as a point source, with no indication of the host galaxy. The host galaxy of 3C 66A was marginally resolved by Wurtz et al. (1996). They found $R_{\rm Gunn} = 19.0^{\rm mag}$ for the host galaxy; the Hubble type could not be determined. In 3C 66A, a weak Mg II emission line has been detected by Miller et al. (1978). This led to the determination of its redshift at $z = 0.444$, which was later confirmed by the detection of a weak Lyα line in the IUE spectrum of 3C 66A (Lanzetta et al. 1993). However, as recently pointed out by Bramel et al. (2005), these redshift determinations are actually still quite uncertain (see also Finke et al. 2008b). In this paper, we do base our analysis on a redshift value of $z = 0.444$, but remind the reader that some results of the physical interpretation should be considered as tentative pending a more solid redshift determination.

The long-term variability of 3C 66A at near-IR (J, H, and K bands) and optical (U, B, V, R, I) wavelengths has recently been compiled and analyzed by Fan & Lin (1999) and Fan & Lin (2000), respectively. Variability at those wavelengths is typically characterized by variations over $\lesssim$1.5 mag on timescales ranging from $\sim$1 week to several years. A positive correlation between the $B-R$ color (spectral hardness) and the R magnitude has been found by Vagnetti et al. (2003). The most recent multiwavelength campaign on 3C 66A in 2003–2004 (Böttcher et al. 2005) found hints for spectral hysteresis, with the $B-R$ hardness peaking several days prior to the R- and B-band fluxes during large flares. This campaign also confirmed the results from an intensive long-monitoring effort by Takalo et al. (1996), revealing evidence for rapid microvariability, including a decline $\sim$0.2 mag within $\sim$6 hr. Lainela et al. (1999) also report a 65 day periodicity of the source in its optically bright state, which has so far not been confirmed in any other analysis. However, the campaign of Böttcher et al. (2005) showed several major outbursts separated by $\sim$50–57 days, possibly also indicating a quasi-periodic behavior.

Superluminal motion of individual radio components of the jet has been detected by Jorstad et al. (2001). While the identification of radio knots across different observing epochs is not unique, Jorstad et al. (2001) favor an interpretation implying superluminal motions of up to $\beta_{\rm app} \sim 19\,h^{-1} \approx 27$, where $h = H_0/(100\ {\rm km\ s^{-1}\ Mpc^{-1}})$ parameterizes the Hubble constant. This would imply a lower limit on the bulk Lorentz factor of the radio emitting regions of $\Gamma \geqslant 27$. Theoretical modeling using a time-dependent leptonic jet model produced an acceptable fit to the SED and light curve of 3C 66A during the 2003–2004 campaign with such a choice of Γ (Joshi & Böttcher 2007).

In the fall of 2007, 3C 66A was found in a very active state, reaching a peak brightness around September 14 of $R \sim 13.4$. This triggered a new optical–IR radio observing campaign by the Whole Earth Blazar Telescope (WEBT)[33] collaboration with

* The radio-to-optical data presented in this paper are stored in the WEBT archive; for questions regarding their availability, contact the WEBT President Massimo Villata (villata@oato.inaf.it).

[33] http://www.oato.inaf.it/blazars/webt/.

Table 1
List of Observatories that Contributed Data to This Campaign[a]

Observatory	Specifications	Frequency/Filters/Energy Range	N_{obs}
	Radio Observatories		
Crimean Radio Obs., Ukraine	22 m	36 GHz	5
Medicina, Italy	32 m	5, 8, 22 GHz	19
Metsähovi, Finland	14 m	37 GHz	32
Noto, Italy	32 m	43 GHz	19
UMRAO, Michigan, USA	26 m	4.8, 8, 14.5 GHz	12
	Infrared Observatories		
Campo Imperatore, Italy	1.1 m	*J*, *H*, *K*	72
	Optical Observatories		
ARIES, Nainital, India	104 cm	*B*, *V*, *R*, *I*	15
Armenzano, Italy	35, 40 cm	*B*, *V*, *R*, *I*	70
Belogradchik, Bulgaria	60 cm	*V*, *R*, *I*	17
Obs. de Bordeaux, France	20 cm	*V*	34
Catania, Italy	91 cm	*U*, *B*, *V*	60
Crimean Astr. Obs., Ukraine	70 cm	*B*, *V*, *R*, *I*	147
Gualba Obs., Spain	35 cm	*V*, *R*, *I*	12
Jakokoski Obs., Finland	51 cm	*R*	69
Kitt Peak (MDM), Arizona, USA	130 cm	*U*, *B*, *V*, *R*, *I*	333
L'Ampolla, Spain	36 cm	*R*	396
Michael Adrian Obs., Germany	120 cm	*R*	180
New Mexico Skies Obs., USA	30 cm	*V*, *R*, *I*	18
Perugia, Italy	40 cm	*R*	25
Roque (KVA), Canary Islands	35 cm	*R*	318
Rozhen, Bulgaria	200 cm	*U*, *B*, *V*, *R*, *I*	139
Sabadell, Spain	50 cm	*V*, *R*	464
San Pedro Mártir, Mexico	84 cm	*R*	10
St. Petersburg, Russia	38 cm	*B*, *V*, *R*, *I*	50
Torino, Italy	105 cm	*B*, *V*, *R*, *I*	77
Tuorla, Finland	103 cm	*R*	19
Valle d'Aosta, Italy	81 cm	*B*, *V*, *R*, *I*	53
Xinglong, China	60 cm	*c*, *i*, *o*	699

Notes. [a] In addition to the standard optical Johnson–Cousin *UBVRIJHK* bands, we obtained optical/near-IR data in the *c*, *i*, and *o* bands. The central wavelengths of these bands are $c = 4206$ Å, $i = 6658$ Å, and $o = 9173$ Å.

intensive monitoring throughout fall and winter 2007–2008. In this paper, we present collected data from late 2007 July through early 2008 March. This high optical state also triggered very high energy γ-ray observations with the VERITAS array. Continued observations by VERITAS throughout the observing season in 2008 resulted in the VHE γ-ray detection mentioned above (Swordy et al. 2008). Details of those observations will be published in a separate paper. In the following, we will present in Section 2 a summary of the observations and data analysis, and present light curves in the various frequency bands. In Section 3, we test for spectral variability to be derived from our results. The cross-correlations between the variability in different optical bands are presented in Section 4. We discuss our results and derive limits on the magnetic field and the Doppler factor in Section 5, and we summarize in Section 6.

Throughout this paper, we refer to α as the energy spectral index, F_ν (Jy) $\propto \nu^{-\alpha}$. A cosmology with $\Omega_m = 0.3$, $\Omega_\Lambda = 0.7$, and $H_0 = 70$ km s^{-1} Mpc^{-1} is used. In this cosmology, and using the redshift of $z = 0.444$, the luminosity distance of 3C 66A is $d_L = 2.46$ Gpc.

2. OBSERVATIONS, DATA REDUCTION, AND LIGHT CURVES

3C 66A was observed in a coordinated multiwavelength campaign at radio, near-IR, and optical frequencies by the WEBT collaboration during the 2007–2008 observing season, from late 2007 July through early 2008 March. The object is being continuously monitored at radio to optical wavelengths by the GLAST-AGILE Support Program (GASP; see Villata et al. 2008), whose observers also contributed to this campaign. The overall timeline of the campaign, along with the measured long-term light curves at radio, infrared, and optical frequencies, is

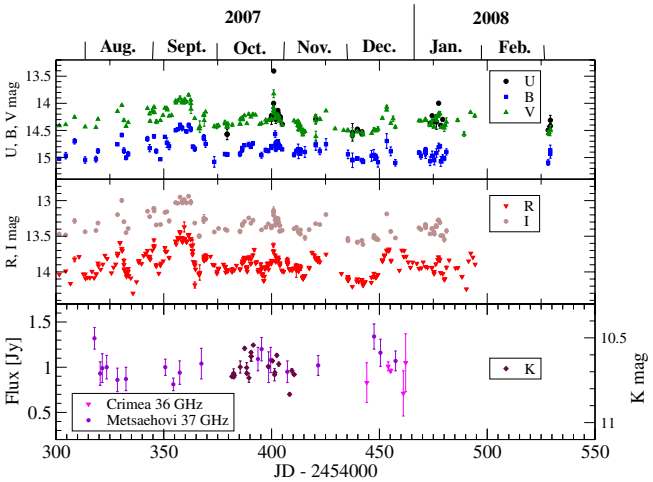

Figure 1. Timeline of the WEBT campaign on 3C 66A in 2007–2008, including the observed (before extinction correction) optical (UBVRI), near-IR *K*-band, and radio light curves.

(A color version of this figure is available in the online journal.)

Table 2
Inter-Instrumental Correction Offsets for Optical Data[b]

Observatory	*B*	*V*	*R*	*I*
ARIES	+0.12	...	...	...
Belogradchik	...	...	...	+0.03
Rozhen	+0.06	...	...	...
Torino	... 0.12	...	...	...
Valle d'Aosta	...	...	...	+0.035

Notes. [b] Only those telescopes are listed for which nonzero offsets were required.

Table 3
Best-fit Parameters of an Asymmetric Gaussian (see Equation (1)) to the Discrete Correlation Functions Between Various Optical Bands

Band (vs. *R*)	*B*	*V*	*I*
F_0	0.703	1.168	0.776
σ_r [d]	2.01 ± 0.51	0.74 ± 0.08	2.02 ± 0.55
σ_d [d]	1.88 ± 0.20	1.28 ± 0.06	2.30 ± 0.27
τ_p [d]	0.13 ± 0.19	-0.01 ± 0.05	0.09 ± 0.21

illustrated in Figure 1. Table 1 lists all participating observatories which contributed data to this campaign. In this section, we will describe the individual observations in the various frequency ranges and outline the data reduction and analysis.

2.1. Optical and Infrared Observations

In the optical component of the WEBT campaign, 22 observatories in 12 countries contributed 3461 individual photometric data points. The observing strategy and data analysis followed to a large extent the standard procedure used for the previous, successful WEBT campaign on 3C 66A in 2003–2004 (Böttcher et al. 2005). Observers were asked to perform bias (and, where necessary, dark) corrections as well as flat fielding on their frames, and obtain instrumental magnitudes, applying either aperture photometry (using IRAF or CCDPHOT) or Gaussian fitting for the source 3C 66A and the comparison star nos. 13, 14, 21, and 23 in the tables of González-Pérez et al. (2001), where high-precision standard magnitudes for these stars have been published. This calibration has then been used to convert instrumental to standard photometric magnitudes for each data set. In the next step, unreliable data points (with large error bars at times when higher-quality data points were available) were discarded. Our data did not provide evidence for significant variability on subhour timescales. Consequently, error bars on individual data sets could be further reduced by rebinning on timescales of 20 min. Finally, there may be systematic offsets between different instruments and telescopes. Wherever our data sets contained sufficient independent measurements to clearly identify such offsets, individual data sets were corrected by applying appropriate correction factors. The resulting offsets, by which individual data sets have been corrected to create a uniform light curve, are listed in Table 2.

In order to provide information on the intrinsic broadband spectral shape (and, in particular, a reliable extraction of $B-R$ color indices), the data were dereddened. For this purpose, Galactic extinction coefficients were calculated using Table 3 of Cardelli et al. (1989), based on $A_B = 0.363$ mag[34] and $R_V = 3.1$. As mentioned in the introduction, the *R* magnitude of the host galaxy of 3C 66A is ∼19 mag, so its contribution

[34] http://nedwww.ipac.caltech.edu/

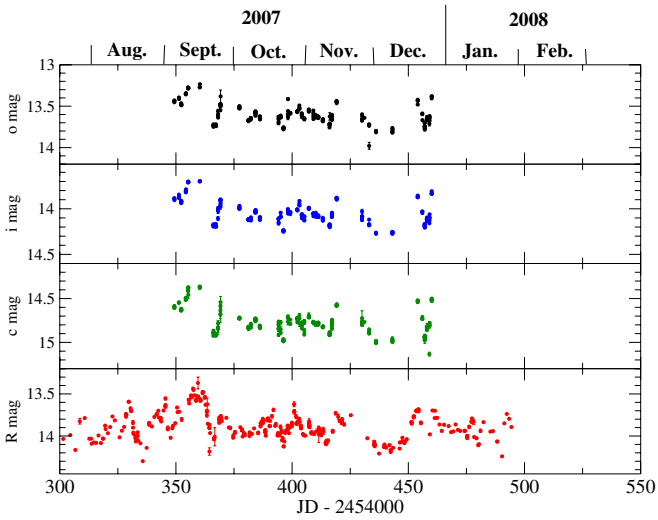

Figure 2. Observed light curves in the optical *R*, *c*, *i*, and *o* bands (before extinction correction) over the entire duration of the campaign. The central wavelengths of these bands are $c = 4206$ Å, $i = 6658$ Å, and $o = 9173$ Å.
(A color version of this figure is available in the online journal.)

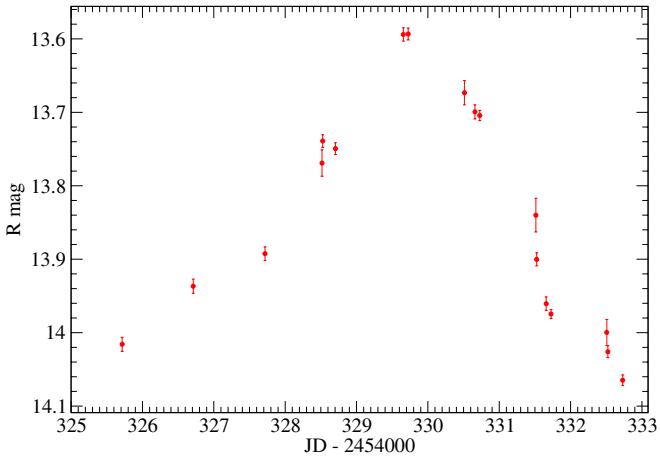

Figure 3. Details of the *R*-band light curve (no extinction correction) during the outburst around 2007 August 16. Particularly remarkable is the rapid decline on JD 2454331 (August 18) with a slope of ∼0.016 mag hr^{-1}.
(A color version of this figure is available in the online journal.)

is negligible compared with the average AGN magnitude of $R \lesssim 14$, and no host-galaxy correction was applied.

As a consequence of the chosen observing strategy, the *R*- and *B*-band light curves are the most densely sampled ones. The *R*-band light curve over the entire duration of the campaign is compared with the light curves at all other optical bands as well as the near-IR *K* band and 36/37 GHz radio light curves in Figures 1 and 2. These figures illustrate that the object remained in a very bright and active state, with an average magnitude of $R \sim 14.0$, throughout the campaign. The source exhibited several large flares with $\Delta R \gtrsim 0.5$ mag out to $R \sim 13.5$–13.6, on characteristic timescales of ∼10 days. The most dramatic outburst occurred around September 14, with a peak magnitude of $R \sim 13.4$. As already found in 2003–2004 (Böttcher et al. 2005), visual inspection of individual major outbursts suggests periods of more rapid decline than rise (see, e.g., Figure 3).

Our campaign revealed clear evidence for rapid intraday microvariability. Two examples are shown in Figures 3 and 4, revealing a rapid decline of the optical brightness by $dR/dt \sim 0.016$ mag h^{-1} on JD 2454331 (2007 August 18), and a rapid rise

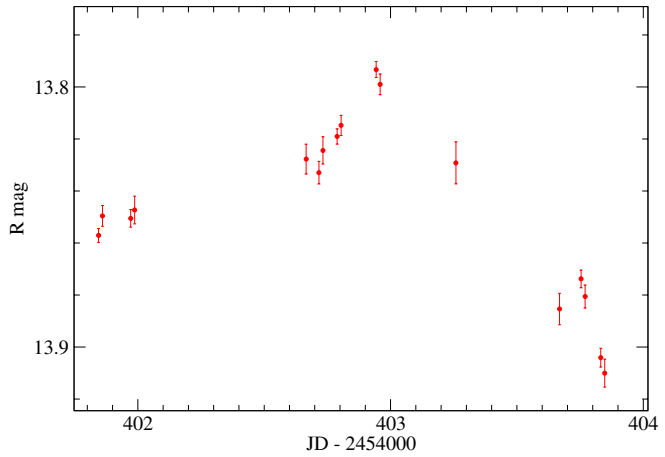

Figure 4. Details of the *R*-band light curve (no extinction correction) on 2007 October 28–29 (JD 2454402–2454403). The rise around JD 2454402.8 has a slope of $\sim$ -0.008 mag hr^{-1}.

(A color version of this figure is available in the online journal.)

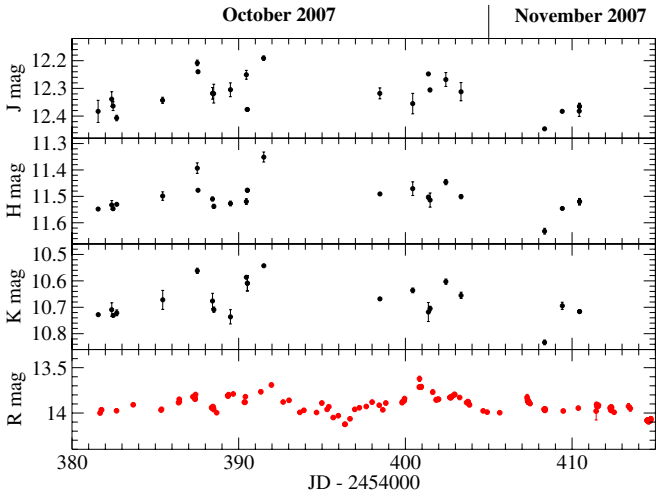

Figure 5. Light curves in the near-IR *J*, *H*, and *K* bands during the campaign, compared to the *R*-band light curve.

(A color version of this figure is available in the online journal.)

by $dR/dt \sim -0.008$ mag hr^{-1} on JD 2454402 (2007 October 28). Our results do not provide any evidence for periodicity or quasiperiodicity. Overall, the variability patterns in all optical bands are very well correlated with no discernable time lag between bands (see Section 4).

In the context of our WEBT campaign, 3C 66A was also observed at near-IR wavelengths in the *J*, *H*, and *K* bands with the AZT-24 1.1 m telescope at Campo Imperatore, Italy. The primary data were analyzed using the same standard technique as the optical data (see above), including flat-field subtraction, extraction of instrumental magnitudes, calibration against comparison stars to obtain standard magnitudes and dereddening. The sampling was not dense enough to allow an improvement of the quality of data by rebinning. Also, the IR observations covered only a period of $\sim$ 1 month so that we cannot draw any conclusions concerning correlated variability with optical or radio fluxes.

The resulting *K*-band light curve is included in Figure 1, and a comparison of all three IR-band light curves (*J*, *H*, *K*) is shown in Figure 5. Within the limited time resolution and coverage, the *JHK* variability tracks the variability in the optical bands. For example, small *BVRI* flares on JD 2454387 and JD 2454391–2454392 are closely matched by the *JHK* light curves. The *JHK* light curves exhibit variability on similar timescales as the optical bands, but with somewhat smaller amplitudes of $\Delta(JHK) \lesssim 0.3$ mag. Rapid variability with rise and decay rates of $\Delta(JHK) \gtrsim 0.1$ mag d^{-1} can be seen, in particular around JD 2454387–2454392.

2.2. Radio Observations

At radio frequencies, the object was monitored using the Noto radio telescope at 43 GHz, the 22 m radio telescope (RT 22) of the Crimean Radio Observatory at 36 GHz, the 26 m telescope of the University of Michigan Radio Astronomy Observatory (UMRAO) at 4.8, 8, and 14.5 GHz, the 14 m Metsähovi Radio Telescope of the Helsinki University of Technology at 37 GHz, and the Medicina radio telescope at 5, 8, and 22 GHz.

The observations at 43 GHz have been performed using the 32 m radio telescope in Noto (Italy). The observations reported in this paper were carried out using the 43 GHz supereterodyne cooled receiver with a 400 MHz instantaneous band. For details of the data analysis and flux calibration, see Ott et al. (1994).

The observations at 36 GHz were carried out at the 22 m Crimean Astrophysical Observatory radio telescope (RT 22), using two similar Dicke switched radiometers. For details of the analysis and calibration of data from the RT 22, see Volvach (2006). At the UMRAO, the source was monitored in the course of the on-going long-term blazar monitoring program. The data were analyzed following the standard procedure described in Aller et al. (1985). As mentioned above, the sampling was rather poor, and some individual errors were rather large due to source confusion problems with 3C 66B.

The 37 GHz observations were made with the 13.7 m diameter Metsähovi radio telescope, which is a radome enclosed paraboloid antenna situated in Finland (24°23′38″E, +60°13′05″). The measurements were made with a 1 GHz-band dual beam receiver centered at 36.8 GHz. A detailed description on the data reduction and analysis is given in Teräsranta et al. (1998).

The radio data at 5, 8, and 22 GHz from the Medicina antenna were taken within a long-term monitoring program of gamma-ray bright blazars. For details on the analysis of data from the Medicina antenna see Bach et al. (2007).

The 36 and 37 GHz light curves from the Crimean Astrophysical Observatory and Metsähovi, respectively, are included in Figure 1 and in the compilation of all radio light curves throughout 2007 in Figure 6. They reveal small-amplitude ($\Delta F/F \lesssim 20\,\%$) variability on timescales of $\sim$10–20 days. The sampling is insufficient to allow any conclusions about possible correlations of the radio variability with optical or infrared variability.

The most dramatic radio variability appears to occur at the highest observed radio frequency of 43 GHz at the Noto radio observatory (see Figure 6), possibly indicating erratic variability on a one-day timescale. However, we point out that the observed erratic variability at higher radio frequencies ($\geqslant$14.5 GHz) may, at least in part, be a consequence of interstellar scintillation (for a more detailed discussion of this aspect, see Böttcher et al. 2005).

3. OPTICAL SPECTRAL VARIABILITY

To investigate the optical spectral variability observed during our campaign, we first computed snapshot optical continuum spectra for several points in time throughout the campaign. A compilation of several such optical/near-IR sections of the SEDs are plotted in Figure 7. As in our earlier campaign on 3C 66A

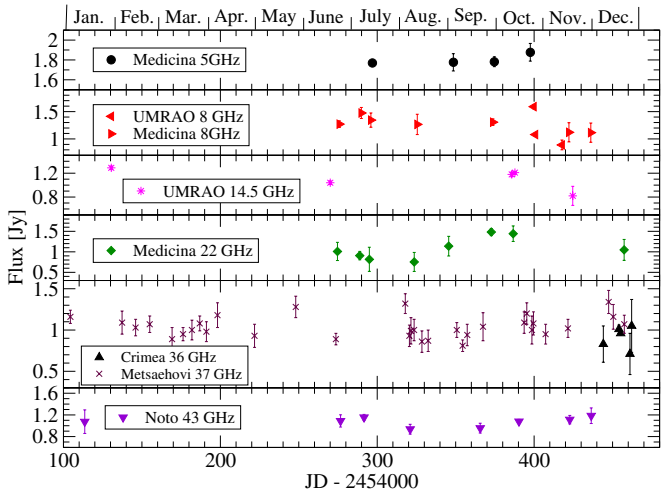

Figure 6. Radio light curves of 3C 66A in 2007.
(A color version of this figure is available in the online journal.)

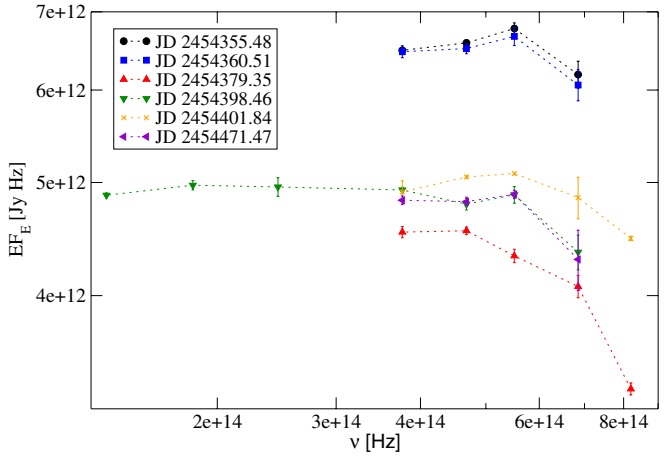

Figure 7. Intrinsic (after extinction correction) optical–near-IR spectral energy distributions during six epochs throughout the campaign.
(A color version of this figure is available in the online journal.)

(Böttcher et al. 2005), we find the (presumably) synchrotron peak of the SED in the optical regime, around (4–6) $\times$ 10^{14} Hz. In order to investigate whether there is a systematic shift of the synchrotron peak with varying optical flux level, we calculated $B-R$ color indices for any pair of B and R magnitude measurements taken within 20 minutes of each other. Figure 8 shows the resulting plot of the $B-R$ color index versus time, together with the R-band light curve. This figure does not confirm the hint in our compilation of snapshot optical/IR SEDs of a correlation between the brightness and the hardness of the source during our campaign.

This is further illustrated in Figure 9, showing the hardness–intensity diagram of $B-R$ color index versus R-band magnitude. No trend of $B-R$ index with brightness can be found. In our previous campaign (Böttcher et al. 2005), we had found a weak positive correlation of hardness with flux for low flux states, $R_{\rm dered} \gtrsim 14.0$ (in agreement with the positive correlation identified by Vagnetti et al. 2003), but no correlation at brighter flux states. Similar results were also found for the LBL BL Lacertae (Papadakis et al. 2007). Since during the entire 2007–2008 campaign the source remained in a bright state with $R_{\rm dered} \lesssim 14.0$, our results are in perfect agreement with our previous findings.

In Böttcher et al. (2005), we had also found hints of systematic spectral evolution during optical flares, with peaks of the $B-R$ hardness occurring consistently a few days before peaks in the R-band light curve. Hardness–intensity diagrams of an individual flare showed a tentative hint of spectral hysteresis. During our 2007–2008 campaign, we did not find such indications. Figure 10 shows the time-resolved hardness-intensity diagram and spectral evolution during the exceptionally bright outburst around 2007 September 15 (~JD 2454348–2454370). The points are labeled by their respective JD, and the arrows indicate the time sequence. Our results do not confirm the existence of spectral hysteresis in 3C 66A.

4. INTERBAND CROSS-CORRELATIONS AND TIME LAGS

Our spectral variability analysis in the previous section already indicated the lack of systematic spectral variability. This would be consistent with a tight correlation at zero time lag between different optical bands. We tested this hypothesis using the discrete correlation function (DCF; Edelson & Krolik 1988).

Figure 11 shows a compilation of the DCFs of the B, V, and I bands with respect to R as a reference band. We calculated DCFs with various time lag bins and obtained consistent results, independent of our choice of the bin size. In order to test for possible time lags between the various light curves, we fitted the DCFs with an asymmetric Gaussian of the form

$$\mathrm{DCF}(\tau) = F_0 \begin{cases} e^{-\frac{(\tau-\tau_p)^2}{\sigma_r^2}} & \text{for } \tau \leqslant \tau_p \\ e^{-\frac{(\tau-\tau_p)^2}{\sigma_d^2}} & \text{for } \tau > \tau_p \end{cases} \quad (1)$$

where F_0 is the peak value of the DCF, τ_p is the delay timescale at which the DCF peaks, and $\sigma_{r,d}$ parametrizes the Gaussian width of the DCF. The best-fit functions are plotted in Figure 11, and the best-fit parameters are quoted in Table 3. These results confirm that there is no evidence for time lags among the optical bands in our campaign data. The rather low normalization of the resulting DCF fits of ~0.7 and ~0.8 in the B versus R and I versus R correlations might be a consequence of uneven sampling with several substantial data gaps in the B and I light curves (see Figure 1).

5. DISCUSSION

The location of the synchrotron peak in the optical regime allows an estimate of a combination of the magnetic field $B \equiv B_G$ G and the Doppler factor $D \equiv 10 D_1$. We follow the approach of Equation (8) in Böttcher et al. (2003). Here, the magnetic field energy density is parametrized as a fraction e_B of the energy density in relativistic leptons. Furthermore, constraining the size of the emission region by the observed variability timescale, $\tau_{\rm var,obs} \equiv 1\, \tau_h$ hr, through $R = c\, \tau_{\rm var,obs}\, D/(1+z)$, we find

$$B_{e_B} = 8.4 \left(\frac{d_{27}^4\, f_{-10}\, e_B^2\, (1+z)^2}{\epsilon_{\rm sy,-6}\, (p-2)\, \tau_h^6\, D_1^{13}} \right)^{1/7} \mathrm{G}, \quad (2)$$

where $d_{27} = 7.38$ is the luminosity distance in units of 10^{27} cm, $f_{-10} \approx 0.5$ is the peak νF_ν flux in units of 10^{-10} erg cm^{-2} s^{-1}, and $\epsilon_{\rm sy,-6} = \epsilon_{\rm sy}/10^{-6} \approx 5$ the dimensionless photon energy, $\epsilon = h\nu/(m_e c^2)$, at the peak of the synchrotron component at $\nu_{\rm sy} \sim 5 \times 10^{14}$ Hz. p is the spectral index of the nonthermal

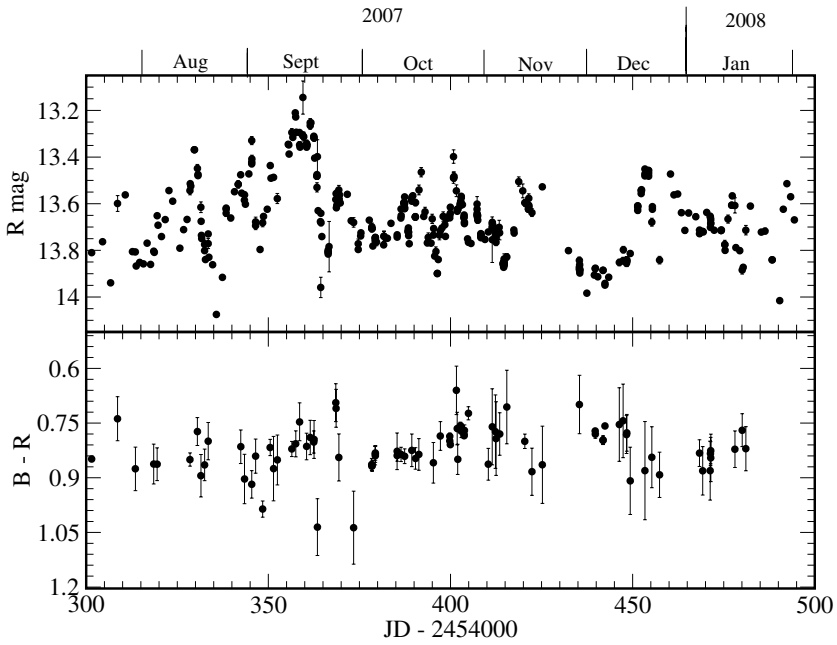

Figure 8. Intrinsic (after extinction correction) light curves of the R magnitudes and the intrinsic $B-R$ color index of 3C 66A over the duration of the entire campaign. No obvious correlation can be identified.

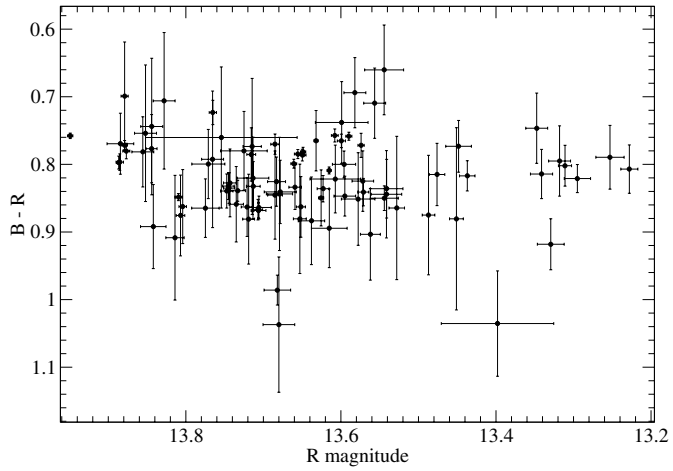

Figure 9. Intrinsic optical hardness–intensity diagram for the complete data set over the entire duration of the campaign. No correlation of the $B-R$ index with R-band magnitude can be identified.

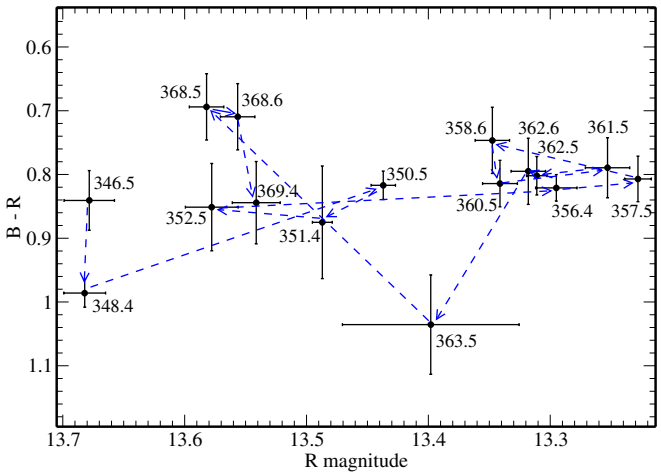

Figure 10. Intrinsic optical hardness–intensity diagram for the flare around 2007 September 15. Individual points are labeled by JD−2454000, and the arrows indicate the time sequence. No hints of spectral hysteresis or other systematic spectral evolution are visible.

(A color version of this figure is available in the online journal.)

electron population radiating above the synchrotron peak. With these values, Equation (2) yields

$$B_{e_B} = 19\, e_B^{2/7}\, (p-2)^{-1/7}\, \tau_h^{-6/7}\, D_1^{-13/7}\ \mathrm{G}. \qquad (3)$$

The lack of spectral variability may be interpreted as evidence that the synchrotron cooling time of electrons radiating in the optical regime is shorter than the light crossing time, which (including a factor $D/(1+z)$) then determines the shortest observed variability timescale. If this were not the case, frequency-dependent radiative cooling effects would be expected to lead to observable time lags and systematic spectral variability. Hence, the condition $\tau'_{\rm sy}\,(1+z)/D \leqslant \tau_{\rm var,obs}$ may be translated into a Doppler-factor-dependent lower limit on the magnetic field. Regarding electrons emitting in the R band, we find

$$\tau_{\rm sy,obs} = 7.32\times 10^4 \left(\frac{1+z}{D}\right)^{1/2} B_G^{-3/2}\ \mathrm{s} \leqslant \tau_{\rm var,obs}, \qquad (4)$$

which yields the magnetic-field limit

$$B \geqslant 3.9\, D^{-1/3}\, \tau_h^{-2/3}\ \mathrm{G}. \qquad (5)$$

Combining this limit with the magnetic-field estimate of Equation (3), we infer an upper limit on the Doppler factor:

$$D \leqslant 28\, (p-2)^{-3/32}\, \tau_h^{-1/8}\, e_B^{3/16}. \qquad (6)$$

This restricts the Doppler factor to values typically found in the modeling of blazar-type quasars and LBLs and excludes extreme values of $\Gamma \sim D \gtrsim 50$, found in one-zone, leptonic

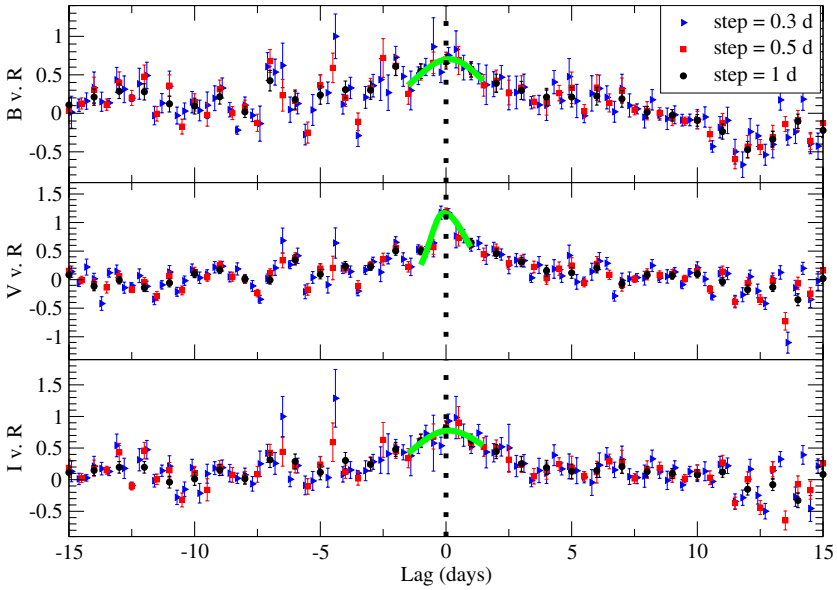

Figure 11. DCFs of *B*, *V*, and *I* band vs. *R*-band light curves. Different symbols indicate different time lag bin sizes, as indicated in the legend, indicating that our results are independent of our choice of a bin size. The curves indicate our best fit with an asymmetric Gaussian.

(A color version of this figure is available in the online journal.)

synchrotron-self-Compton models for several HBLs detected at $E \gtrsim 1$ TeV (e.g., Begelman et al. 2008; Ghisellini & Tavecchio 2008; Finke et al. 2008a). This aspect is particularly exciting now, after the recent detection of 3C 66A at greater than 100 GeV energies by VERITAS (Swordy et al. 2008). The very high Doppler factors mentioned above are primarily required to accommodate the very rapid variability, on timescales down to just a few minutes, at GeV–TeV energies seen in a few HBLs. Should future VHE γ-ray observations of 3C 66A indicate such rapid variability for this object as well, this would pose serious problems for conventional blazar emission models.

6. SUMMARY

We reported on an extensive optical, near-IR (*JHK*), and radio monitoring campaign by the WEBT throughout the fall and winter of 2007–2008, prompted by a high optical state in 2007 September with $R < 13.5$. 28 observatories in 12 countries in North America, Europe, and Asia contributed to this campaign.

The source remained in a high optical state throughout the observing period and exhibited several bright flares on timescales of ∼10 days, including an exceptional outburst around 2007 September 15–20, reaching a peak brightness at $R \sim 13.4$. Our campaign revealed microvariability with flux changes up to $|dR/dt| \sim 0.02$ mag hr^{-1} with occasional indications of a slower rise than decay of individual flares.

Our observations do not reveal evidence for systematic spectral variability in the overall high state ($R_{\rm dered} \lesssim 14.0$) covered by our campaign, in agreement with previous results for the same overall brightness state. Note, however, that a positive correlation between optical spectral hardness ($B-R$ color index) and optical flux at dereddened *R*-band magnitudes of $R_{\rm dered} \gtrsim 14.0$ has been found before. In particular, we do not find evidence for spectral hysteresis in 3C 66A for which hints were found in an earlier campaign in a somewhat lower flux state. On the same note, we did not find evidence for time lags between optical bands.

During our campaign, as in earlier campaigns, the peak of the low-frequency (presumably synchrotron) component of the SED of 3C 66A was located in the optical regime. From the observed synchrotron peak flux, we infer a value of the magnetic field of the emission region of $B \sim 19\, e_B^{2/7}\, \tau_h^{-6/7}\, D_1^{13/7}$ G. From the lack of systematic spectral variability, a Doppler-factor-dependent lower limit on the magnetic field can be derived, which implies an upper limit on the Doppler factor, $D \leqslant 28\, \tau_h^{-1/8}\, e_B^{3/16}$. This excludes extreme values of the Doppler factor of $D \gtrsim 50$, inferred for some HBLs detected at TeV energies.

The work of M. Böttcher was partially supported through NASA's *XMM-Newton* guest observer program, award NNX08AD67G. The UMRAO is partially supported by funds from the NSF, most recently AST-0607523, and from the University of Michigan's Department of Astronomy. This publication is partly based on observations with the Medicina and Noto telescopes operated by INAF-Istituto di Radioastronomia. The Metsähovi radio astronomy team acknowledges support from the Academy of Finland. J.W. and X.Z. are supported by the Chinese National Natural Science Foundation grants 10603006, 10573020, and 10633020. The AZT-24 observations were made within an agreement between the Pulkovo, Rome, and Teramo Observatories.

REFERENCES

Acciari, V. A., et al. (The VERITAS Collaboration) 2008, ApJ, 634, L73
Aharonian, F., et al. 2007, ApJ, 664, L71
Albert, J., et al. 2007a, ApJ, 666, L17
Albert, J., et al. 2007b, ApJ, 669, 862
Albert, J., et al. 2008, Science, 320, 1752
Aller, M. F., Aller, D. H., & Hughes, P. A. 1994, in Tuorla Observatory Reports 174, Workshop on Intensive Monitoring of OJ 287, Orilampi, Finland, June 17–20, ed. M. R. Kidger & L. O. Takalo, 60
Aller, H. D., Aller, M. F., Latimer, G. E., & Hodge, P. E. 1985, ApJS, 59, 513
Bach, U., et al. 2007, A&A, 464, 175
Begelman, M. C., Fabian, A. C., & Rees, M. J. 2008, MNRAS, 384, L19

Böttcher, M. 2007, ApSS, 309, 95
Böttcher, M., et al. 2003, ApJ, 596, 847
Böttcher, M., et al. 2005, ApJ, 968, 977
Bramel, D. A., et al. 2005, ApJ, 629, 108
Cardelli, J. A., Clayton, C., & Mathis, J. S. 1989, ApJ, 345, 245
Costamante, L., & Ghisellini, G. 2002, A&A, 384, 56
Edelson, R. A., & Krolik, J. H. 1988, ApJ, 333, 646
Fan, J. H., & Lin, R. G. 1999, ApJS, 121, 131
Fan, J. H., & Lin, R. G. 2000, ApJ, 537, 101
Finke, J. D., Dermer, C. D., & Böttcher, M. 2008b, ApJ, 686, 181
Finke, J. D., Shields, J. C., Böttcher, M., & Basu, S. 2008a, A&A, 477, 513
Ghisellino, G., & Tavecchio, F. 2008, MNRAS, 386, L28
González-Pérez, J. N., Kidger, M. R., & Martín-Luis, F. 2001, AJ, 122, 2055
Jorstad, S. G., Marscher, A. P., Mattox, J. R., Wehrle, A. E., Bloom, S. D., & Yurchenko, A. V. 2001, ApJS, 134, 181
Joshi, M., & Böttcher, M. 2007, ApJ, 662, 884
Lainela, M., et al. 1999, ApJ, 521, 561
Lanzetta, K. M., Turnshek, D. A., & Sandoval, J. 1993, ApJS, 84, 109
Miller, J. S., French, H. B., & Hawley, S. A. 1978, in Pittsburgh Conference on BL Lac Objects, ed. A. M. Wolfe (Pittsburgh, PA: Univ. Pittsburgh), 176
Mücke, A., & Protheroe, R. J. 2001, Astropart. Phys., 15, 121
Mücke, A., Protheroe, R. J., Engel, R., Rachen, J. P., & Stanev, T. 2003, Astropart. Phys., 18, 593
Ott, M., Witzel, A., Quirrenbach, A., Krichbaum, T. P., Standke, K. H., Schalinski, C. J., & Hummel, C. A. 1994, A&A, 284, 331
Papadakis, I., et al. 2007, A&A, 470, 857
Swordy, S., et al. 2008, ATel, 1753
Takalo, L. O., et al. 1996, A&AS, 120, 313
Teräsranta, H., et al. 1998, A&AS, 132, 305
Vagnetti, F., Trevese, D., & Nesci, R. 2003, ApJ, 590, 123
Villata, M., et al. 2008, A&A, 481, L79
Volvach, A. E. , in ASP Conf. Ser. 360, AGN Variability from X-Rays to Radio Waves, ed. C. Martin Gaskell, I. M. McHardy, B. M. Peterson, & S. G. Sergeev (San Francisco, CA: ASP), 133
Wills, B. J., & Wills, D. 1974, ApJ, 190, L97
Wurtz, R., Stocke, J. T., & Yee, H. K. C. 1996, ApJS, 103, 109